Temporal structure of stimulated-Brillouin-scattering reflectivity considering transversal-mode development

Shahraam Afshaarvahid,[1,*] Axel Heuer,[2,†] Ralf Menzel,[2] and Jesper Munch[1]

[1]*Department of Physics and Mathematical Physics, Adelaide University, SA 5005, Australia*

[2]*Lehrstuhl für Photonik, Universität Potsdam, Am Neuen Palais 10, 14469 Potsdam, Germany*

The time-resolved reflectivity of optical phase conjugation by stimulated Brillouin scattering (SBS) is investigated both theoretically and experimentally. A three-dimensional and transient model of SBS is developed to compare the experimental and theoretical results. Noise initiation of the SBS process is included in the model to simulate the shot-to-shot variation in the reflectivity and the Stokes temporal profile.

I. INTRODUCTION

Optical phase conjugation by stimulated Brillouin scattering (SBS) has been extensively studied, both theoretically and experimentally, and used in laser systems to improve beam quality since the early 1970s. Extensive experimental studies of SBS have revealed many aspects of this phenomenon and SBS now is used in commercial laser systems. The limitations of the SBS are, by now, well known. However, in spite of all of the extensive theoretical studies [1–16], a single unified numerical model that can include all aspects of SBS phenomena especially transient and transverse effects has not, until recently [17], been developed. Thus, no single model has been able to produce results in good agreement with experiments, even for simple cases such as the temporal profile of the Stokes output or the reflectivity curve. To the best of our knowledge a detailed comparison with a good agreement between the SBS experiment and theory has not been published before.

In this paper we present a detailed comparison of results from our transient three-dimensional model [17] and experiments performed in identical-parameter regime. SBS experiments were carried out using two materials with extreme phonon lifetimes, Freon 113 with $\tau=0.84$ ns and SF_6 with $\tau=17.4$ ns. The total reflectivity vs input energy and the temporal profile of the Stokes output were examined experimentally and numerically. An excellent agreement between the experimental and numerical results has been achieved.

II. THEORY

The equations describing the SBS process are derived from Maxwell's equations for the electric fields and the Navier-Stokes equation for the acoustic field inside the material. Using the slowly varying envelope approximation, the three-dimensional transient-SBS equations describing the acoustic, Stokes and pump fields propagating along the z direction, can be written as [18,19,12]

$$\left(\frac{\partial}{\partial t}+\Gamma\right)Q=-ig_1E_lE_s^*, \tag{1a}$$

$$\left(\frac{i}{2k_s}\nabla_t^2+\frac{n}{c}\frac{\partial}{\partial t}+\frac{\partial}{\partial z}\right)E_s=-ig_2Q^*E_l, \tag{1b}$$

$$\left(\frac{-i}{2k_l}\nabla_t^2+\frac{n}{c}\frac{\partial}{\partial t}-\frac{\partial}{\partial z}\right)E_l=-ig_2QE_s. \tag{1c}$$

Here ∇_t^2 refers to the derivatives in the transverse directions x and y, g_1 and g_2 are coupling constants given by

$$g_1=\frac{\omega^2\gamma n}{\pi\omega_q c^2},$$

$$g_2=\frac{\omega\gamma}{4cn\rho_0},$$

n is the refractive index of the medium and $k_s\approx k_l$ are the Stokes and pump wave numbers, respectively. In the transverse directions, we use a decomposition method [20,4,5,11,14] to expand the electric fields in terms of orthonormal bases modes A_m and B_m,

$$E_l(\mathbf{r}_\perp,z,t)=\sum_m a_m(z,t)A_m(\mathbf{r}_\perp,z), \tag{2}$$

$$E_s(\mathbf{r}_\perp,z,t)=\sum_m b_m(z,t)B_m(\mathbf{r}_\perp,z), \tag{3}$$

where $\mathbf{r}_\perp$ is the position vector in transverse directions and the particular set of A_m and B_m used in our model will be given below. By substituting Eqs. (2) and (3) into Eqs. (1a)–(1c) and assuming that A_m and B_m satisfy the homogeneous Maxwell equations, Eqs. (1b) and (1c) can be rewritten as [17]

$$\left(\frac{n}{c}\frac{\partial}{\partial t}+\frac{\partial}{\partial z}\right)b_n=g_1g_2\sum_{i,j,k}C_{ij}^*a_kg_{knij}, \tag{4}$$

$$\left(\frac{n}{c}\frac{\partial}{\partial t}-\frac{\partial}{\partial z}\right)a_n=-g_1g_2\sum_{i,j,k}C_{ij}b_kg_{knij}^*, \tag{5}$$

*Electronic address: shahraam@physics.adelaide.edu.au

†Electronic address: heuer@rz.uni-potsdam.de

where

$$C_{ij}(z,t)=\int_0^t [a_i(z,\tau)b_j^*(z,\tau)+f_{ij}(z,\tau)]e^{-\Gamma(t-\tau)}d\tau \quad (6)$$

$$g_{knij}=\int_{-\infty}^{+\infty} A_i^* A_k B_j B_n^* d^2r, \quad (7)$$

and f_{ij} in Eq. (6) are Langevin noise terms that simulate the thermal noise initiation of SBS process. They are usually chosen [21,8] such that they have spatial and temporal Gaussian distribution and are δ correlated in the sense that

$$\langle f_{ij}(z,t)f_{kl}^*(z',t')\rangle=Q_0\delta_{ik}\delta_{jl}\delta(z-z')\delta(t-t'), \quad (8)$$

where the constant Q_0 is given by Ref. [21] as

$$Q_0=\frac{2kT\rho_0\Gamma}{g_1^2 v^2}. \quad (9)$$

Here k is the Boltzman constant, T is the temperature, ρ_0 is mean density, and v is the velocity of sound in the material. Q_0 determines the strength of the fluctuations in f [21].

In our model, we use an uncorrelated Gaussian distribution for f and consider the variance of f, i.e. σ^2, as a free parameter. The value of this free parameter is set by finding the best fit between the numerical and experimental results for the SBS reflectivity curve. Once a σ^2 has been found for a material, it is kept constant.

In Eqs. (4) and (5), obtained for any general form of A_i and B_j, the only term that depends on the form of A_i and B_j is the tensor $g_{knij}=\int_{-\infty}^{+\infty}A_i^* A_k B_j B_n^* d^2r$. Our model can thus equivalently be developed for any kind of orthonormal bases A_i and B_j. Since we are interested in the phase conjugation properties of SBS we chose the complex conjugate of A_n as the basis for the Stokes wave, i.e., $B_n(\mathbf{r}_\perp,z)=A_n^*(\mathbf{r}_\perp,z)$. This enables us to examine how much of the energy in a particular input mode is reflected as the conjugated mode. For the basis A_n, we have examined the cylindrically symmetric Laguerre-Gaussian functions used by Miller *et al.* [5] as [22]

$$A_n(r,z)=\left(\frac{2}{\pi}\right)^{1/2}\frac{1}{\omega(z)}e^{i(n+1/2)\psi(z)}L_n\left(\frac{2r^2}{\omega(z)^2}\right)$$

$$\times\exp\left[-i\frac{kr^2}{2R(z)}-\frac{r^2}{\omega(z)^2}\right], \quad (10)$$

where the spot size $\omega^2(z)$, radius of curvature $R(z)$, and Gouy phase angle $\psi(z)$ are given by the usual expressions,

$$\omega^2(z)=\omega_0^2\left[1+\left(\frac{z}{z_R}\right)^2\right], \quad R(z)=z+\frac{z_R^2}{z},$$

$$\psi(z)=\tan^{-1}\left(\frac{z}{z_R}\right), \quad (11)$$
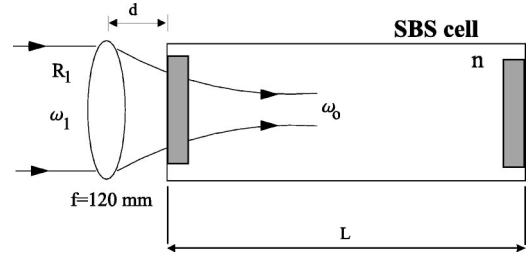

FIG. 1. Focusing geometry used in the SBS experiments and modeling.

and $r=|\mathbf{r}_\perp|=\sqrt{x^2+y^2}$. As usual, the Rayleigh range z_R is related to the beam waist radius ω_0 (for the fundamental mode) and wave length λ as $z_R=\pi\omega_0^2 n/\lambda$, where ω_0 is related to the input fundamental beam radius ω_1 and radius of curvature R_1 (see Fig. 1). Utilizing the expressions for the basis A_n, Eq. (10), the integral in Eq. (7) can be evaluated as

$$g_{knij}=\int_{-\infty}^{+\infty} A_i^* A_k B_j B_n^* d^2r$$

$$=\frac{\exp[i(k+n-i-j)\psi(z)]}{\omega(z)^2}\varepsilon_{knij}, \quad (12)$$

where ε_{knij} is a symmetric real tensor given by the overlap integral

$$\varepsilon_{knij}=\left(\frac{2}{\pi}\right)\int_0^{+\infty}dx e^{-2x}L_k(x)L_n(x)L_i(x)L_j(x). \quad (13)$$

The gain tensor g_{knij} depends on the phase mismatch factor $\exp[i(k+n-i-j)\psi(z)]$ and the mode-coupling constant ε_{knij}. It will be shown that the overall gain of any mode is entirely determined by these two factors. Some values of ε_{knij} are shown in the Table I. In our model we have solved Eqs. (4) and (5) numerically [17].

III. EXPERIMENTAL AND NUMERICAL RESULTS

The experimental layout is shown in Fig. 2. A passive q-switched Nd:YAG (yttrium-aluminum-garnet) laser operat-

TABLE I. Numerical values of ε_{knij}.

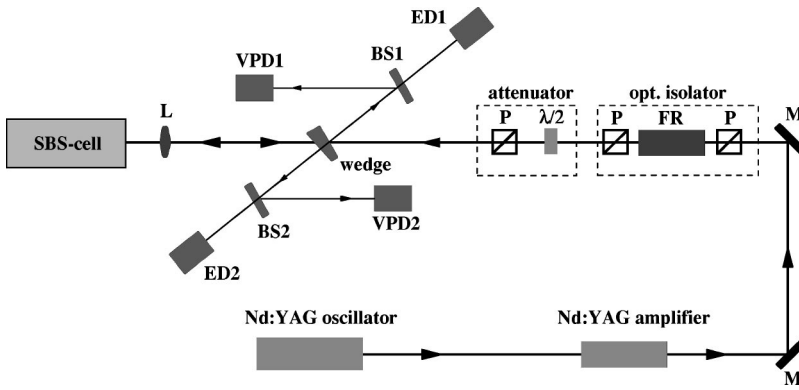| k	i	j	n	ε_{knij}
0	0	0	0	0.3183
0	0	0	1	0.1592
0	0	1	1	0.1592
0	1	1	1	0.0796
1	1	1	1	0.1592
1	1	1	2	0.0796
1	1	2	2	0.0995
1	2	2	2	0.0547
2	2	2	2	0.1094
2	2	2	3	0.0547
2	2	3	3	0.0746
3	3	3	3	0.0846

FIG. 2. The Experimental layout of the SBS process.

ing at $\lambda = 1064$ nm was used as pump beam source. The laser emits pulses with a duration of about 30 ns at a repetition rate of 20 Hz. All pulses were longitudinal and transverse single mode (TEM00) with vertical polarization. The single longitudinal mode operation was achieved with an intracavity, 10-mm-thick quartz Fabry-Perot etalon. The spectral bandwidth of the pulses was about 100 MHz. With an additional amplifier the pulse energy could be increased up to 50 mJ. The laser was isolated from the reflected light by a polarizer, a Faraday rotator followed by a second polarizer. To attenuate the pulse energy continuously a combination of a half-wave retardation plate and a polarizer was used. A wedge was applied as a beamsplitter for measuring both the incident and the reflected radiation. The energy of the input and the reflected pulse was detected by two identical energy detectors (Laserprobe RJP 637). As diagnostics for the temporal pulse shapes two vacuum photodiodes with 100-ps rise time and a Tektronix digital oscilloscope (1 GHz bandwidth) were used.

The SBS materials used were Freon 113 and SF_6 for both experiment and numerical modeling. A near-Gaussian beam ($M^2 = 1.4$) was focused into the SBS cell.

A. Freon 113

The SBS reflectivity and the temporal profiles of the Stokes pulses for the SBS process were examined experimentally and numerically, using a SBS cell filled with Freon 113. The experimental and numerical parameters include (Fig. 1): cell length $L = 200$ mm, focal length $f = 120$ mm, distance between the lens and the entrance window $d = 45$ mm, input radius of curvature $R_1 = 2403$ mm, input beam radius $\omega_1 = 1.45$ mm, phonon lifetime 0.84 ns, gain of the medium 0.0062 cm/MW, index of refraction, $n = 1.36$, and entrance window thickness 2 mm (BK7).

The SBS reflectivity was measured as a function of energy from below to high above the threshold energy. In the SBS experiment, the reflectivity of SBS at a given energy showed variation from shot to shot due to noise initiation of the SBS process. In our model, we ran the computer code ten times with different initial noise distribution and take the mean value of reflectivity for each energy. Figure 3 shows the experimental and numerical reflectivity results for the SBS process using Freon 113. The numerical results were fitted to the experimental results by selecting the value of the

free parameter σ^2. The numerical result in Fig. 3 (solid line) is obtained for $\sigma = 2.79 \times 10^{-8}$ MW s^2/cm^5. Although this value gives good agreement between the numerical and the experimental results at mid and high energies, the numerical result is slightly higher than the experimental results at low energy, e.g., $E \sim 6$ mJ in Fig. 3. This may indicate that the strength of the initial noise distribution $Q_0 \propto 2AkT\rho_0\Gamma/g_1v^2$ is not constant for the whole range of input energies. For example, at high energies the temperature of the liquid is higher resulting in a larger σ than the low energies. Once the value of σ was chosen, we used it to examine the temporal profile of the Stokes return. The simulation was run 20 times with different initial noise distributions and for three different energies, 11 mJ, 21 mJ, and 43 mJ. Due to different initial noise, each of the 20 output Stokes returns had slightly different temporal profiles. The Stokes temporal profiles are shown in Fig. 4. The solid lines in the figure are experimental results and the dotted lines are the numerical model results of 20 Stokes pulses. The experimental and numerical input pulses are the same and are shown in the figure.

For the numerical model we have assumed that the input pulse is a perfect zero-order Gaussian in the transverse direction, i.e.,

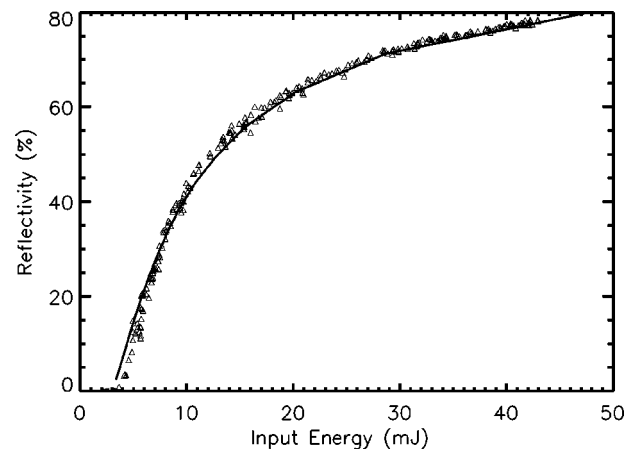$$E_l(\mathbf{r}_\perp, z, t) = a_0(z,t)A_0(\mathbf{r}_\perp, z).$$

FIG. 3. The reflectivity of the SBS process in Freon 113 as a function of energy. There is a good agreement between the numerical (solid line) results and the experimental (triangles).
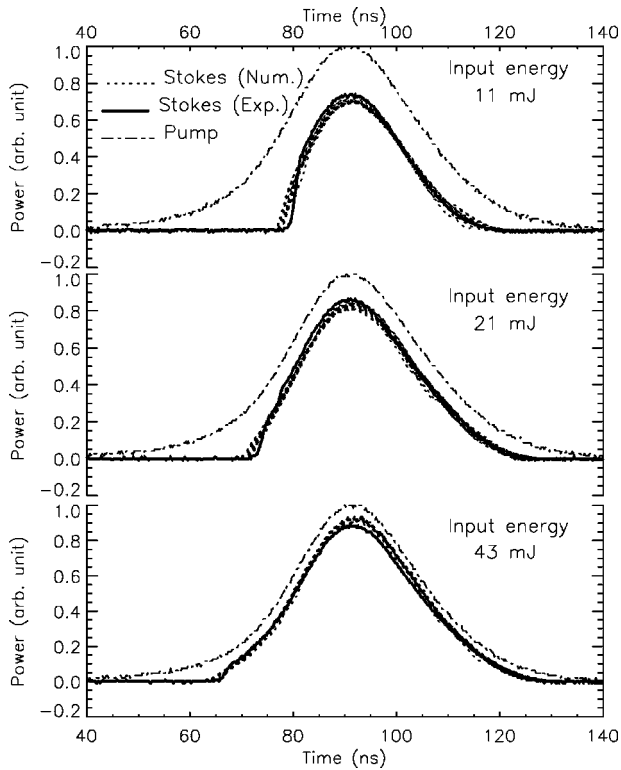
FIG. 4. Temporal profiles of the input and output (Stokes) pulses in the SBS experiment in Freon 113. The dotted lines are numerical results (20 pulses) and the solid lines are the experimental results.

This input pulse, however, initiates all the other transverse modes in the Stokes return and they all contribute to the output energy. The energy carried by each transverse mode of the Stokes field decreases for higher-order modes. For example, examining one of the numerical output Stokes pulses for the case of 11-mJ input pulse, Fig. 4, reveals that how higher-order transverse modes contribue to the total output Stokes pulse, Fig. 5. Calculating the energy contained in each transverse mode in Fig. 5, we find that about 80% of the total output energy is carried by the zero transverse mode
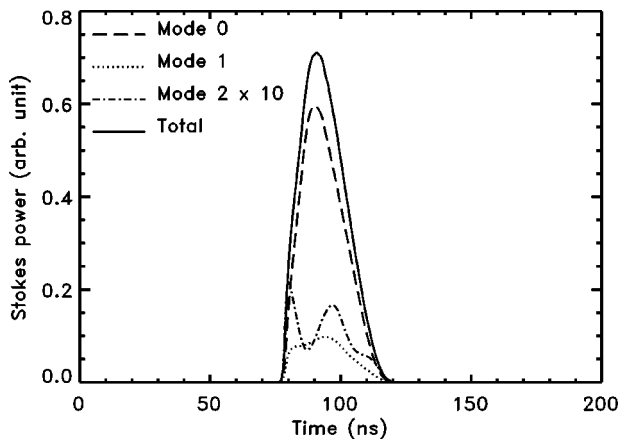

FIG. 5. Temporal profiles of the different transverse modes of the Stokes pulse. Higher modes of the Stokes pulse contribute in carrying the output energy.
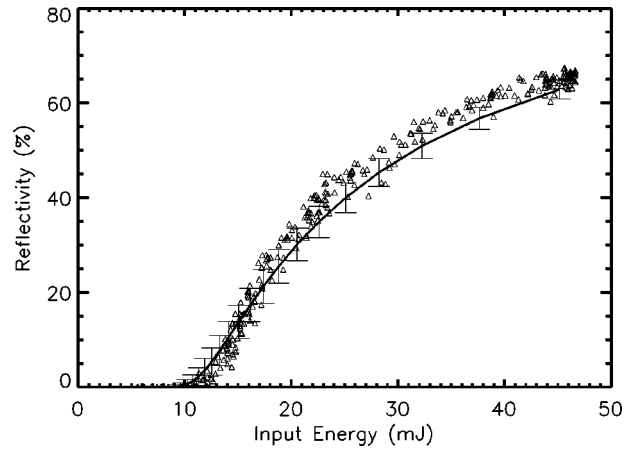

FIG. 6. The reflectivity of the SBS process in SF_6 as a function of energy. There is good agreement between the numerical (solid line) results and the experimental (triangles).

and the remaining 20% of the output energy is carried as 15.6% in mode 1, 2.6% in mode 2, and 1.8% in higher-order modes. These results could be used as an indication of theoretical fidelity of the phase conjugation process of about 80% in this case (roughly speaking the fraction of Stokes energy that is carried by the zero mode of Stokes pulse). The distribution of output energy among the different transverse modes of the Stokes pulse was found to be a function of the
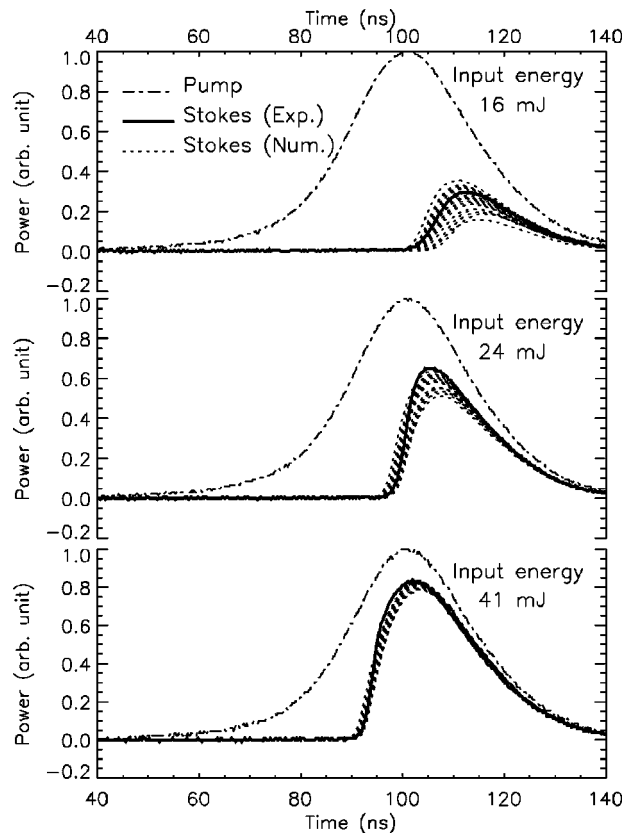

FIG. 7. Temporal profiles of the input and output (Stokes) pulses in the SBS experiment in SF_6. The dotted lines are numerical results (20 pulses) and the solid lines are the experimental results.

input energy. For higher input energies, the fraction of energy in the zero-order mode increases, indicating better fidelity.

B. SF$_6$

Using a SBS cell filled with SF$_6$, we have examined experimentally and numerically the reflectivity and the Stokes temporal profile in the SBS process. We used pure SF6 at a pressure of 20.5 bar with the following geometrical and material parameters (Fig. 1): cell length $L = 139$ mm, focal length $f = 120$ mm, distance between the lens and the entrance window $d = 45$ mm, input radius of curvature $R_1 = 2403$ mm, input beam radius $\omega_1 = 1.6$ mm, phonon lifetime 17.3 ns, gain of the medium 0.014 cm/MW, index of refraction, $n = 1.023$, and entrance window thickness 2 mm (BK7)

The SBS reflectivity was measured as a function of input energy as shown in Fig. 6. The calculated value of the reflectivity was obtained from the average of ten simulation using different initiation noise. The comparison between the numerical and experimental results is shown in Fig. 6. The solid line in Fig. 6 shows the mean value of reflectivity obtained from numerical calculations. The error bars in the figure, calculated using the numerical code, show the range of

reflectivity for each energy. The free parameter σ that gives the best fit with the experimental data for SF$_6$ is $\sigma = 1.194 \times 10^{-8}$ MW s^2/cm^5. A trend, similar to that of the Freon results (Fig. 3) can be seen in Fig. 6: the initial noise strength σ should be bigger for high input energies. As for Freon, the temporal profiles of the output Stokes pulses at three different energies were measured and compared with the corresponding numerical results. Again, the numerical results in each case included 20 pulses, which were obtained by running the computer code for 20 different initial noise distributions. The results in Fig. 7 show a good agreement between the experimental and numerical results.

IV. DISCUSSION

A numerical model of SBS that includes both transverse and transient effects was used in an accurate comparison with SBS experiment. An excellent agreement was obtained for SBS reflectivity and for temporal profiles of the Stokes output as functions of input energies. With this initial confirmation of the model, it can now, with confidence, be used for laser-system simulations, or be further developed. For instance, the model can be developed to include astigmatic or short coherence length input laser beams.

---

[1] C.L. Tang, J. Appl. Phys. **37**, 2945 (1966).

[2] R.H. Lehmberg, J. Opt. Soc. Am. **73**, 558 (1983).

[3] M.J. Damzen and H. Hutchinson, IEEE J. Quantum Electron. **19**, 7 (1983).

[4] P. Suni and J. Falk, J. Opt. Soc. Am. B **3**, 1681 (1986).

[5] E.J. Miller, M.D. Skeldon, and R.W. Boyd, Appl. Opt. **28**, 92 (1989).

[6] E.M. Dianov, A.Y. Karasik, A.V. Lutchnikov, and A.N. Pilipetskii, Opt. Quantum Electron. **21**, 381 (1989).

[7] P.H. Hu, J.A. Goldstone, and S. Ma, J. Opt. Soc. Am. B **6**, 1813 (1989).

[8] A.L. Gaeta and R.W. Boyd, Phys. Rev. A **44**, 3205 (1991).

[9] R. Menzel and H.J. Eichler, Phys. Rev. A **46**, 7139 (1992).

[10] R. Chu, M. Kanefsky, and J. Falk, J. Appl. Phys. **71**, 4653 (1992).

[11] A. Kummrow, Opt. Commun. **96**, 185 (1993).

[12] R. Chu, M. Kanefsky, and J. Falk, J. Opt. Soc. Am. B **11**, 331 (1994).

[13] E. Kuzin, M. Petrov, and A. Fotiadi, *Principles of Phase Conjugation* (Springer-Verlag, Berlin, 1994).

[14] T.R. Moore and R.W. Boyd, J. Nonlinear Opt. Phys. Mater. **5**, 387 (1996).

[15] S. Afshaarvahid, V. Devrelis, and J. Munch, Phys. Rev. A **57**, 3961 (1998).

[16] T.R. Moore, G.L. Fischer, and R.W. Boyd, J. Mod. Opt. **45**, 735 (1998).

[17] S. Afshaarvahid and J. Munch, J. Nonlinear Opt. Phys. Mater. **10**, (2001).

[18] W. Kaiser and M. Maier, in *Laser Handbook*, edited by F. T. Arecchi and E. O. Schuls-Dubis (North-Holland, Amsterdam, 1972), Vol. 2, pp. 1077-1149.

[19] G.C. Valley, IEEE J. Quantum Electron. **22**, 704 (1986).

[20] I.Y. Anikeev, I.G. Zubarev, and S.I. Mikhailov, Sov. Phys. JETP **57**, 978 (1983).

[21] R.W. Boyd, K. Rzazewski, and P. Narum, Phys. Rev. A **42**, 5514 (1990).

[22] A. E. Siegman, *Lasers* (University Science Books, Mill Valley, CA, 1986).